Rochín-Bañaga, H., Davis, D.W., and Schwennicke, T., 2021, First U-Pb dating of fossilized soft tissue using a new approach to paleontological chronometry: Geology, v. 49,https://doi.org/10.1130/G48386.1

First U-Pb dating of fossilized soft tissue toward practical paleontological chronometry

Heriberto Rochín-Bañaga[1*], Donald W. Davis[1], and Tobias Schwennicke[2]
[1]*Department of Earth Sciences, University of Toronto, 22 Russell Street, Toronto, ON M5S 3B1, Canada.*
[2]*Departamento de Ciencias de la Tierra, Universidad Autónoma de Baja California Sur, La Paz, Km. 5.5, B. C. S. 23080, México.*

SUPPLEMENTAL DATA

ANALYTICAL METHODS

Backscattered electron (BSE) imaging was done using a JEOL JSM6610-Lv scanning electron microscope at the Department of Earth Sciences, University of Toronto, to identify the mineral phases in the mold. The U-Pb isotopic analyses were conducted at the University of Toronto using an Agilent 7900 ICPMS and an NWR193 excimer laser system. U-Pb data were collected using scan-lines over samples, resulting in hundreds of cycle data per line. The path of each line, 3-5 mm long, was pre-ablated at a fast scan rate using a larger diameter beam in order to remove surface contamination. Since the laser only penetrates a few microns into the sample, we can exclude bias due to downhole fractionation. U-Pb line analyses were conducted with laser frequency of 193 nm, fluence of about 4.5 J/cm^2 and frequency of 10 Hz at a rate of 20 microns/sec. Six scan-lines on the mold were done on the phosphatic matrix whereas the scan-lines on the shark teeth were done on their roots. For the phosphatized mold the laser beam diameter was 50 µm, for the shark teeth, 25-50 µm, and for the phosphatic clasts, 50 µm. Baselines were accumulated on each scan for 15 sec prior to opening the laser.

Over the course of the project, it was discovered that the ablation system showed a significant dependence of oxide level with position along the X (left to right) axis of the sample in the chamber. The problem was found to be due to leakage of helium around 3 small O-ring seals on the stainless-steel tube that conducts the helium carrier gas out of the ablation chamber. The NWR193 ablation chamber moves to position samples beneath the laser. The He gas tube position is fixed relative to the laser so the exit hole in the ablation chamber slides along it when the X coordinate of the sample is changed. Leakage was found to increase with the X value (movement of the ablation chamber to the left positioning samples toward the right side underneath the laser). No sample is lost but the reduction in helium flow has the same effect as a reduction in carrier argon gas, which is to reduce the total flow of gas into the plasma torch, thereby reducing advection of air into the plasma and oxidation of the sample. Variable oxidation causes variable loss of U signal due to formation of UO^+, but does not affect the Pb signal. If the

X coordinate values of the sample and standard are significantly different, this will introduce a bias in measured $^{206}Pb/^{238}U$ due to different oxidation levels. We note this problem because similarly designed ablation chambers are widely used in the community so the problem may be affecting data elsewhere. It is recommended that oxygen levels in the signal be monitored during analysis by including measurement of mass ^{34}O (molecular $^{16}O^{18}O$) in the ablation parameters. This signal is normally roughly 100K c/s and can be precisely measured with a 10 msec dwell time. If any sulphur is present in samples, the oxide level can be determined from baseline measurements. Oxides can also be monitored using mass 56 ($^{40}Ar^{16}O$), but this is a much larger signal and overlaps with ^{56}Fe. If a variation in baseline ^{34}O signal is observed with position, the O-ring seals on the metal He gas exit tube should be replaced. Data in this work were measured after this problem was resolved.

Glass standards NIST610 and NIST612 were used to correct for mass and elemental oxide fractionation bias between each U-Pb measurement. Measured $^{206}Pb/^{238}U$ bias on NIST612 is consistently higher than that on NIST610 by 2.5% when they are run together. NIST612 standard was run against the Madagascar apatite standard MAD2. The age of the MAD2 apatite was measured at 474 Ma by isotope dilution TIMS (Thomson et al. 2012), assuming a $^{207}Pb/^{206}Pb$ ratio of initial common Pb of 0.87 as predicted by the Stacey and Kramers (1975) Pb evolution model for average crust. As shown in Supplementary Data Fig. S1, constraining the common-radiogenic Pb mixing line through the data at an initial $^{207}Pb/^{206}Pb$ (Y-intercept) value of 0.87 gives the same age as with TIMS. Therefore, no standard bias correction is made to ages measured using NIST612. Ages measured using NIST610 were multiplied by a factor of 1.026 to correct for fractionation bias between the two glasses.

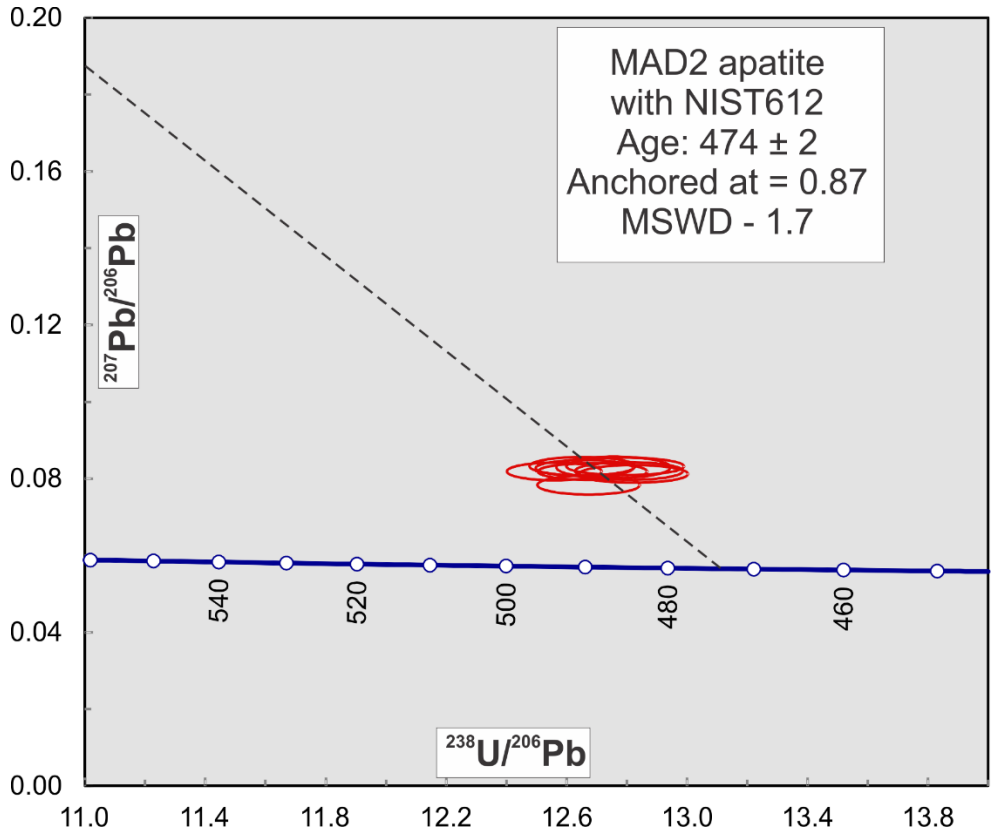

Figure S1. U-Pb analyses of the MAD2 apatite standard calibrated against NIST612 glass. The best-fit line is forced through an initial $^{207}Pb/^{206}Pb$ ratio of 0.87.

REFERENCES CITED

Stacey, J.S., and Kramers, J.D., 1975, Approximation of terrestrial lead isotope evolution by two stage model: Earth and Planetary Science Letters, v. 26, p. 207–221, https://doi.org/10.1016/0012-821X(75)90088-6.

Thomson, S.N., Gehrels, G.E., Ruiz, J., and Buchwaldt, R., 2012, Routine low-damage apatite U-Pb dating using laser ablation–multicollector–ICPMS: Geochemistry, Geophysics, Geosystems, v. 13, Q0AA21, https://doi.org/10.1029/2011GC003928.

Table S1: U-Pb ages results from fossil samples in the Salada Fm., Baja. Mexico

Sample	^{238}U ppm	^{206}Pb ppm	^{232}Th ppm	Th/U	UtilChron				Isoplot				
									T-W		Weth		
					Age (Ma)	95% Err	PbC	95% Err	Age (Ma)	95% Err	Age (Ma)	95% Err	MSWD
Mold (six lines)	202.8	0.7	0.7	0.0037	3.16	0.08	0.817	0.004	3.36	0.08	3.15	0.08	1.0
Mold (Line 1)	142.0	1.2	1.1	0.0080	2.85	0.18	0.813	0.006	3.26	0.19	2.82	0.18	1.0
Mold (Line 2)	211.0	1.1	0.7	0.0032	3.42	0.54	0.816	0.018	3.79	0.54	3.42	0.54	0.8
Mold (Line 3)	177.5	0.4	0.9	0.0048	3.04	0.45	0.812	0.025	3.35	0.45	3.04	0.45	0.9
Mold (Line 4)	262.7	0.7	0.4	0.0014	3.22	0.14	0.827	0.015	3.41	0.14	3.21	0.14	1.1
Mold (Line 5)	201.9	0.3	0.3	0.0014	3.02	0.29	0.788	0.033	3.12	0.29	3.00	0.29	0.7
Mold (Line 6)	221.9	0.6	0.8	0.0036	3.15	0.19	0.808	0.014	3.30	0.19	3.17	0.18	0.7
Shark tooth 1	731.9	4.1	0.2	0.0003	3.00	0.24	0.842	0.009	3.15	0.25	2.98	0.24	0.8
Shark tooth 2	156.4	2.7	0.9	0.0055	2.06	0.35	0.822	0.005	2.51	0.35	2.06	0.35	0.5
Shark tooth 3	302.0	0.8	1.9	0.0063	0.93	0.30	0.835	0.018	1.16	0.30	0.93	0.29	1.0
Shark tooth 4	437.0	4.2	1.8	0.0042	2.70	0.26	0.840	0.008	3.12	0.26	2.70	0.26	0.8
Shark tooth 5	62.9	0.2	0.01	0.0002	2.05	0.38	0.838	0.015	2.53	0.39	2.04	0.39	0.9
Shark tooth 6	104.7	0.4	0.03	0.0003	1.75	0.38	0.831	0.016	2.21	0.39	1.75	0.38	0.9
Extraclast 1	37.0	1.0	0.7	0.0179	5.43	1.62	0.847	0.014	7.80	2.00	4.30	2.00	1.5
Extraclast 2	53.6	1.1	1.1	0.0212	4.58	1.59	0.853	0.014	5.90	2.10	5.60	2.00	1.5
Extraclast 3	32.7	0.6	0.9	0.0263	5.38	1.96	0.847	0.021	6.60	2.00	5.40	1.90	1.1

PbC - 207Pb/206Pb of common Pb component
UtilChron - Bayesian 2D regression
T-W - Tera-Wasserburg calculation
Weth - Wetherhill calculation
MSWD - Mean square of weighted deviations